Field Simulation Technique to Enhance Mechanical Behavior and Elemental Composition of Soft Clay Soil using Thermal Treatment

Ali H. Shareef [*] , Mohammed A. Al-Neami , Falah H. Rahil

Posted Date: 29 November 2023

doi: 10.20944/preprints202311.1881.v1

Keywords: bearing ratio; settlement ratio; heating; spacing; depth; CPT; EDS

Article

Field Simulation Technique to Enhance Mechanical Behavior and Elemental Composition of Soft Clay Soil Using Thermal Treatment

Ali H. Shareef *, Mohammed A. Al-Neami and Falah H. Rahil

Civil Engineering Department, University of Technology, Iraq; 40008@uotechnology.edu.iq (M.A.A.-N.); 40029@uotechnology.edu.iq (F.H.R.)

* Correspondence: bce.20.36@grad.uotechnology.edu.iq

Abstract: Clay covers a substantial portion of the Earth. Such soil covers Iraq's central and southern regions, where the depth of the clay may reach 150 m. All enhancement techniques and methods for transporting large loads cease to function or become prohibitively expensive in such soils. In this case, thermal treatment is the most effective method. In this study, a novel heating system was created and produced utilizing gas as the heat source via boreholes that simulate reality. The borehole heating cases were planted inside soft clay soil to enhance the soil. Different parameters were investigated, including the spacing between boreholes (3, 4, and 5 times the outer diameter of the borehole), the heating depth (1, 1.5, 2, and 2.5 times the width of the model footing), the duration of heating (2, 4, 6, 8, and 10 hrs), and the pattern (square, circular, triangular). The results showed the strength and behavior of the soil treated with heated boreholes at varying spacings, depths, patterns, and heating periods. The best results were found for a spacing, depth, and heating time of three times the outer diameter of the borehole, two times the width of the footing model, and eight hours, respectively. The effect of the heated borehole casing pattern was small when the heated borehole casing was used. The experiments conducted on heated soil showed that the undrained shear strength (Cu) increased from 14 to 360 kPa and then dropped to 140 kPa (as an average with depth). In contrast, the average angle of internal friction (Ø) rose from 0 to 52 degrees and decreased to 16 degrees (as an average with depth) from the center of the heating model to the furthest point affected by heating. In addition, the EDS pattern showed that components like silicon, aluminum, and iron dropped at 300 °C and rose at 400 °C in the treated soils. At 200 °C, the calcium content rose, and then dropped dramatically at 400 °C. The carbon percentage increased at 300 °C and decreased at 400 °C. The elements' proportions showed little change or remained stable at temperatures between 400 °C and 600 °C.

Keywords: bearing ratio; settlement ratio; heating; spacing; depth; CPT; EDS

1. Introduction

A low bearing capacity and extensive expected subsidence are the primary issues associated with weak soil, as well as the stability of constructions built on such soils [1]. Soft clayey soil, which is frequently encountered in civil engineering projects, is one of the problematic soil types that occupies a significant portion of the globe, such as many lowlands and coastal regions, where industrial and urban centers are located [2]. High plasticity, dispersivity, high compressibility, swelling, excessive settlement, low strength, and susceptibility to environmental variables are some of the most significant strength and behavioral difficulties related to certain types of soil [3]. Generally, all problematic soils should be modified to enhance their behavior and strength [4]. Based on the treatment approach, engineering methods for ground modification can be roughly divided into three categories: chemical, biological, and mechanical stability. Thermal treatment is a technique utilized for improving the behavior and strength of weak soils. Several studies on the impact of high temperatures on soil quality have been published in recent years. Ref. [5] examined the influence of

 doi:10.20944/preprints202311.1881.v1

heating on different types of fine soils in the east of Turkey and discovered that the degree of heating (20 to 1000 °C) significantly affected the clay's characteristics, such as specific gravity, maximum dry density, and optimal water content. Ref. [6] examined the effect of the degree of heating (20 to 400 °C) on three types of fine loose soil in the north of Jordan in laboratory circumstances and discovered that heat enhancement decreased the plasticity index, optimal moisture content, pressure of swelling, and undrained shear strength of the soil. Ref. [7] researched clay heated at 200–800 °C in a heating furnace to study the development of the clay's physical characteristics under high-temperature heating. At high temperatures, the clay was shown to be influenced by three primary processes, including chemical alterations in the mineral composition, heat-induced microcracking, and fractures in the mineral particles. Through laboratory measurements, the researchers in [8] studied the effect of the degree of heating (20 °C (room temperature) to 900 °C) on the thermophysical characteristics of clay and determined that, after heating, clay's thermal conductivity exhibits a strong linearity with density. Ref. [9] utilized microwave heating to strengthen a weak clayey insertion in specimens and found that when the temperature rose higher than 500 °C, the soil's water stability significantly improved, and the treatment using microwaves also increased the cracks and porosity of the fine soil inside, making it suitable for grout reinforcement. Ref. [10] examined the potential of microwave sintering to improve radioactively polluted soil and found that it may be an effective remediation method for radioactive soil pollutants. Ref. [11] developed a custom high-temperature device to heat soft clay soil at 105 °C, 150 °C, and 200 °C and found that the duration of heating affected the dry density, saturation, and volume change in the sample in a nonlinear pattern. Ref. [12] examined the thermo-consolidation properties of soft clay soil in the Ningbo region, China, by conducting thermo-consolidation experiments at varying temperatures and confining pressures and found that a higher temperature increased the degree of consolidation. Ref. [13] determined a mathematical equation for the variation in the angle of internal friction and cohesion with temperature by examining the effects of the confining pressure, dry density, and water content on the effectiveness of the swelling soil. Ref. [14] explored how temperature affected the dielectric properties of kaolin specimens exposed to microwave radiation and found that the existence of surface transporters that absorb microwave electromagnetic fields is correlated with a high efficiency of the heating action. The application of heated microwaves has the apparent ability to alter the swelling properties of expansive soil, with the vertical free swelling strain and the free swelling ratio of the soil samples decreasing substantially following microwave heating; their relationship with microwave heating duration is close to linear after approximately fifteen minutes of heating in microwaves, after which the soil sample may become hardened and cease to qualify as expansive soil [15]. According to the above-mentioned research, the temperature and exposure duration are crucial parameters influencing soils' qualities. However, in terms of heat treatment, soil samples are typically subjected to inefficient high-temperature furnaces. Regarding the heat treatment of clay soils, particularly soft clay soils in locations where long-term engineering projects are expected to be created, a heating system and bearing load device have been invented that accurately represent field conditions. Due to Iraq's abundant oil and gas reserves, the heating system was designed to run on cooking gas. Therefore, this research aimed to study the effect of the heat treatment approach using a heated borehole surrounded by soft clay soil. This research also revealed the strength and behavior of the soil treated using heated boreholes with varying spacings, depths, patterns, and heating periods that simulated reality. In addition, the bearing capacity parameter values for the thermally treated soils were determined using an electrical cone penetration probe (CPT) with a cross-sectional area of 1000 mm^2, under ASTM D 5778. Finally, energy-dispersive spectroscopy (EDS) diffraction testing was conducted to compare the chemical change in the treated and untreated soils.

2. Methodology and Experimental Work

2.1. Materials Used

This study used three materials: soil, gas, and water. The soil sample used in this study was brought from the Al-Amer site in Baghdad city. The physicochemical properties of the soil are listed

Preprints (www.preprints.org) | NOT PEER-REVIEWED | Posted: 29 November 2023 doi:10.20944/preprints202311.1881.v1

in Table 1, and the soil particle size distribution is illustrated in Figure 1. The LPG used in the study was domestic compressed gas inside a cylinder, consisting mainly of methane and including propane, ethane, and heavier hydrocarbons. The gas also provides trace amounts of nitrogen, hydrogen sulfide, carbon dioxide, and water, which burn in a mixture of around 4% to 12% air by volume [16]. Lastly, tap water was used in the experiment.

Table 1. Physicochemical properties of soil.

Index Property	Index Value
Liquid Limit (%)	45
Plastic Limit (%)	23
Plasticity Index (%)	22
Specific Gravity	2.69
Gravel %	0
Sand %	2
Silt %	20
Clay %	78
Classification (USCS)	CL
Organic Matter (%)	<0.01
Total Dissolved Salt (%)	2.21
pH Value	7.2

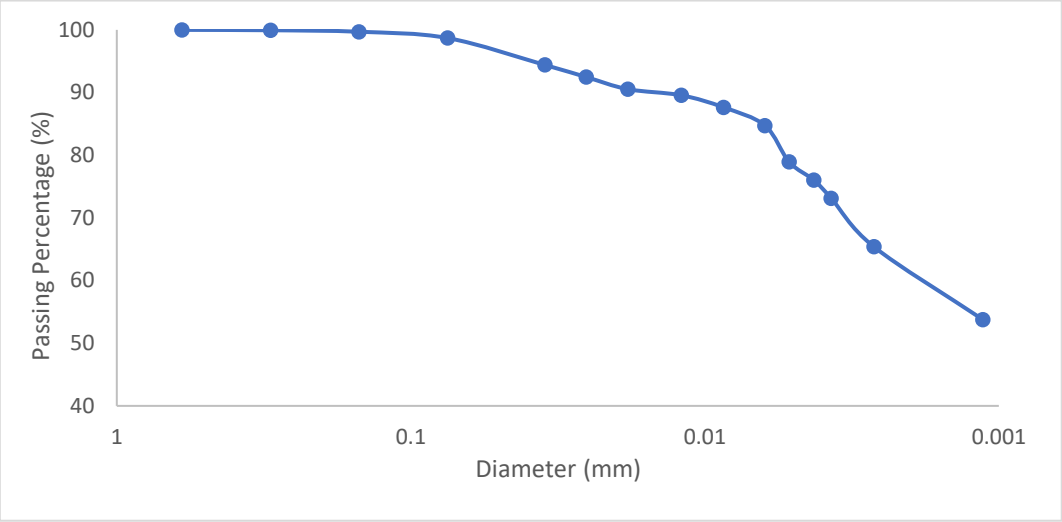

Figure 1. Grain size of soil.

2.2. Devices and Tests Used in This Study

In order to explore the response of heated soft clay soil, it is crucial to simulate circumstances similar to those that may be encountered in the field. A specific piece of testing apparatus and its attachments were created and constructed to accomplish this objective. The devices provide heating, and then a monotonic load is applied to a 200 × 200 mm^2 area for the model foundation. The evaluation system includes the following components: metal load framework, metal box, casing (barrier tube), and heating system.

2.2.1. Metal Load Framework

A metal structure was created to sustain the verticality of the piston mechanism used to deliver the center-focused load onto the treated soil inside a metal box with interior dimensions (92.5 × 92.5 × 92.5) cm^3, and it bore the penetration motor of the borehole casing throughout the heating process, as shown in Figure 2.

Preprints (www.preprints.org) | NOT PEER-REVIEWED | Posted: 29 November 2023 doi:10.20944/preprints202311.1881.v1

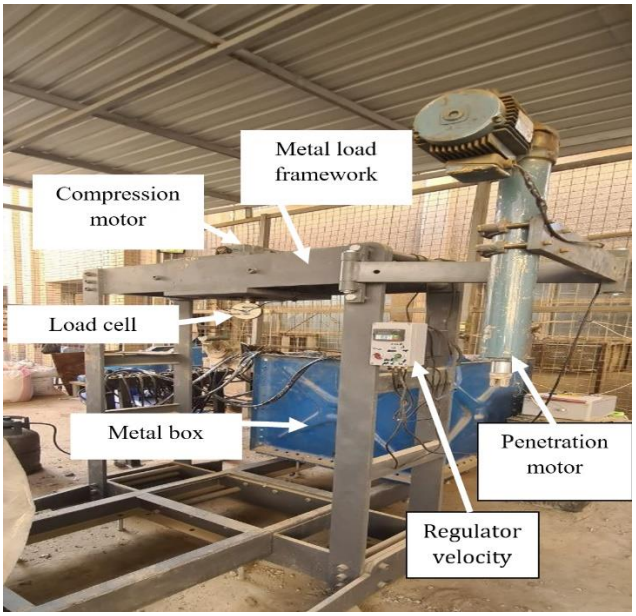

Figure 2. Metal load framework.

2.2.2. Casing (Barrier Tube)

The casing for the borehole was manufactured using four sizes of carbon steel according to A53 ASTM grade B, with a 43 mm outer diameter and 4 mm thickness. Table 2 presents the physical properties of these cases. Various lengths (1, 1.5, 2, and 2.5 times the width of the model footing) were employed. The four varieties are shown in Figure 3. A previous experimental determination established that a minimum diameter of 35 mm is required to generate fire within the soil [17].

Figure 3. Tube casing of the borehole.

Table 2. Physical properties of pipe casing.

Property	Value
Density at 20 °C (kg/dm^3)	785
Thermal conductivity at 20 °C (W/m K)	50
Specific thermal capacity at 20 °C (J/kg K)	460

2.2.3. Heating System

The heating system was fabricated and installed to create heat inside the soil model. The system is composed of five major components: combustion pipes; rubber pipelines (W/BP 20/30 BAR) that transmit gas and air from the source to the priming pipes; a controller for the heating source; an air compressor that provides the heating system with air, along with a gas bottle and gas regulator; and the measuring devices for the heating system (Figure 4). Two devices are used to measure the temperature. The first is a heat control board with a plastic box holding two temperature controllers that monitor the soil's internal temperature through a thermal connection. These temperature sensors

Preprints (www.preprints.org) | NOT PEER-REVIEWED | Posted: 29 November 2023 doi:10.20944/preprints202311.1881.v1

are 15 and 30 cm in length, have two electric switches to activate the temperature controller, and two electric lamps. The second device uses five thermal sensors linked by a thermal wire spread out within the soil to measure the soil temperature during heating. These sensors' lengths are equal to 30 cm. In addition, the sensors are linked to a data-logger-type Ordel 100 device that records the temperature in the computer. To ensure the accuracy of the results, two models were created for each variable, with the first model containing seven thermal sensors and the second containing two sensors.

Figure 4. Heating system: (**A**) combustion pipes, (**B**) heating source controller, (**C**) heating system measuring devices, and (**D**) air compressor, gas bottle, and gas regulator.

2.2.4. CPT Probe Device

This investigation determined the bearing capacity parameter values for the thermally modified soils using an electrical cone penetration probe (CPT) with a 1000 mm^2 cross-sectional area, as per ASTM D 5778. The influence of overburden pressure resulting from the shallow penetration depth was disregarded. Figure 5 illustrates that the penetrating motor was linked to this probe via a standard adapter. The penetration probe's 10 mm/s velocity remained consistent due to the shallow penetration level.

 doi:10.20944/preprints202311.1881.v1

Figure 5. Preparing the CPT probe to model the test.

2.3. Establishing the Soil Modeling and Test Procedure

An undrained shear strength of 14 kPa was used with 29% water per 25 kg of dry clay soil, where the vane shear, a portable device, was used to achieve an undrained shear strength of the soil equal to 14 kPa. A 120 L laboratory mixer was used for blending. The soil was sealed in polythene bags for one day after mixing to obtain uniform moisture content. Afterwards, the soil was deposited 10 cm deep for each layer in a (92.5 × 92.5 × 92.5) cm^3 metal container and gently crushed with a 60 mm × 60 mm wooden tamper to remove air. After the final layer, the top surface was cleaned and leveled, and a hardwood platform with the same surface area as the bed's soil was placed on the bed with 5 kPa of sitting pressure for one day. After removing the seat pressure, the guide plate was placed according to a different pattern, spacing, and length of the nine borehole cases to complete the installation of those cases; a motor that penetrated using a controlled velocity was used, and then an Auger with a 34.5 cm diameter was used to empty the soils from inside the cases. After this step, the guide plate and motor were removed from the soil model and prepared for heating. The heating pipes (combustion hands) started the heating stage. After inserting the casing into the soil and arranging the gas and air ratio (10% gas, 90% air), the heating system was activated and the heat began to pass from the casing to the soil. Pipe primers ignited the casing fire.

After the operation, the heating equipment was switched off, and the soil model was allowed to reach ambient temperature after 24 h. After preparing the test model, the 20 cm × 20 cm footing was placed in the middle of the soil surface. The metal box was moved to align the foundation, and the motor pressurized the centers with a loading rate of (1 mm/min). Then, the loading transducer and LVDT were installed. Failure was defined as the load being sufficient to induce a settlement equal to 10% of the footing width; although the influence of water vapor that escapes from the top layer causes massive cracks to occur in this layer, a 2 cm (10% of the footing width) depth settlement is a very weak criterion in this state. So, in this research, all models addressed a settlement equal to 15% of the footing width caused by the failure load. Figure 6 shows the stages of preparation of the soil model for the heat treatment and the load test.

Preprints (www.preprints.org) | NOT PEER-REVIEWED | Posted: 29 November 2023 doi:10.20944/preprints202311.1881.v1

Figure 6. Stages of the test procedure for heat treatment and load test.

2.4. Testing Program

The research approach used in this study was constrained to a series of five sequential processes including the analysis of physical models, as shown in Figure 7.

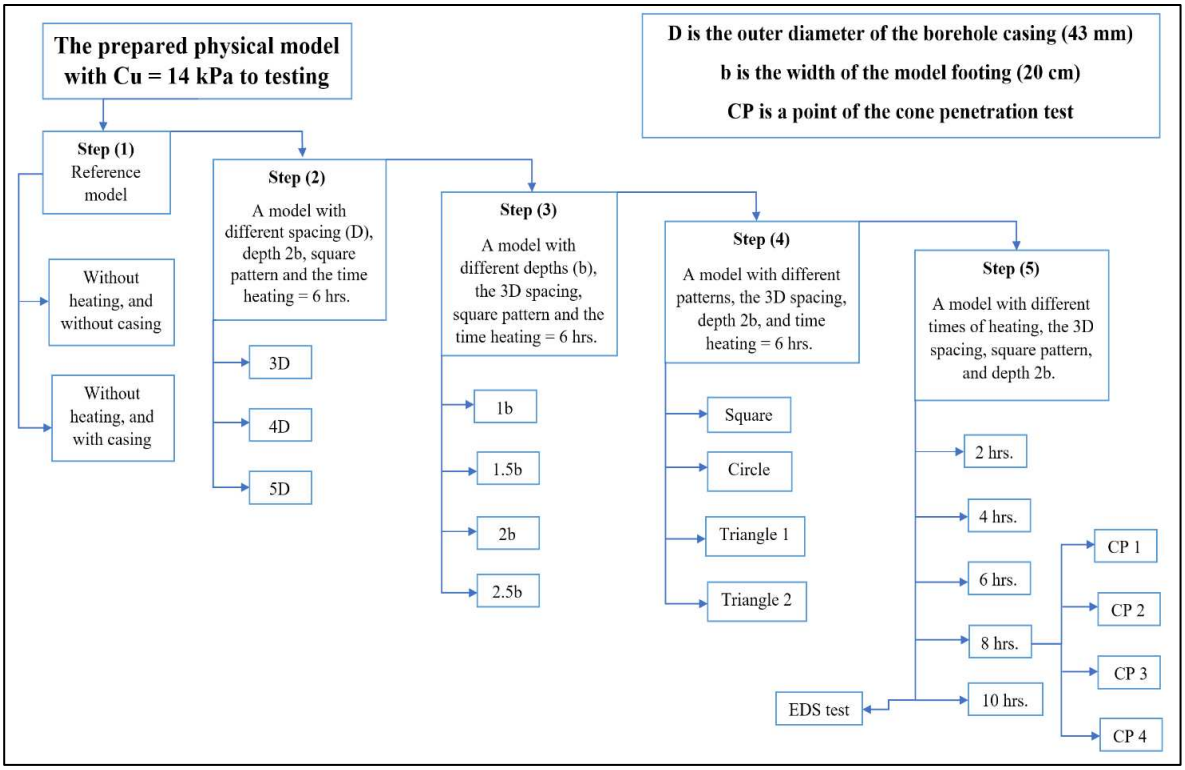

Figure 7. Flowchart of the testing program.

Preprints (www.preprints.org) | NOT PEER-REVIEWED | Posted: 29 November 2023 doi:10.20944/preprints202311.1881.v1

3. Presentation and Discussion of Test Results

3.1. Impact of Distance between Borehole Casing (Spacing)

Three models were executed with nine square patterns of heating boreholes of 40 cm depth (2b), with 3D (13 cm), 4D (17 cm), and 5D (22 cm) as the distance between each borehole. Each model was subjected to six hours of heating. The connection was dimensionless between the bearing ratio (q_u/Cu) and the settlement ratio (Settl./$b_{footing}$) for all models, as shown in Figure 8. The values of the bearing ratio (q_u/Cu) rise when the heating system works and decrease if the distance between the heating boreholes grows up to a space of 5D, where the values of the bearing ratio at the 15% settlement ratio are 5.03, 5.35, 27.26, 24.84, and 21.78 for the models U.W (untreated soil without casing), U.C (untreated soil with casing), 3D, 4D, and 5D, respectively. For spacing increases greater than 3D, such as 4D and 5D, the interlocking between the unit cells is significant and leads to lower temperatures in the center of the treated zone, followed by low values for the bearing ratio, as shown in Figure 9. When the spacing is narrow, as in the 3D model, the unit cells become increasingly interlocked, and the temperature is higher than between the 4D and 5D models, as seen in Figures 10 and 11 (the mechanical properties and chemical changes caused by heating are discussed in the last section).

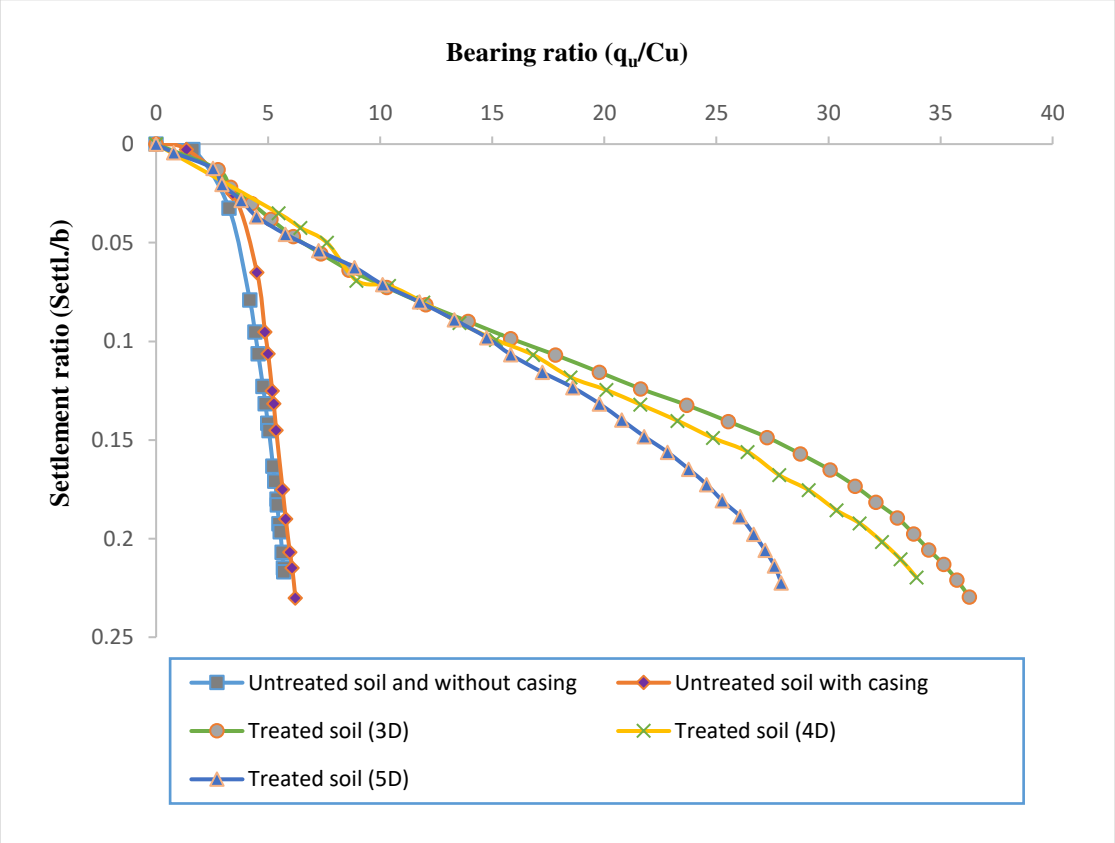

Figure 8. Dimensionless connection between the bearing ratio and the settlement ratio for various spacing models.

Preprints (www.preprints.org) | NOT PEER-REVIEWED | Posted: 29 November 2023 doi:10.20944/preprints202311.1881.v1

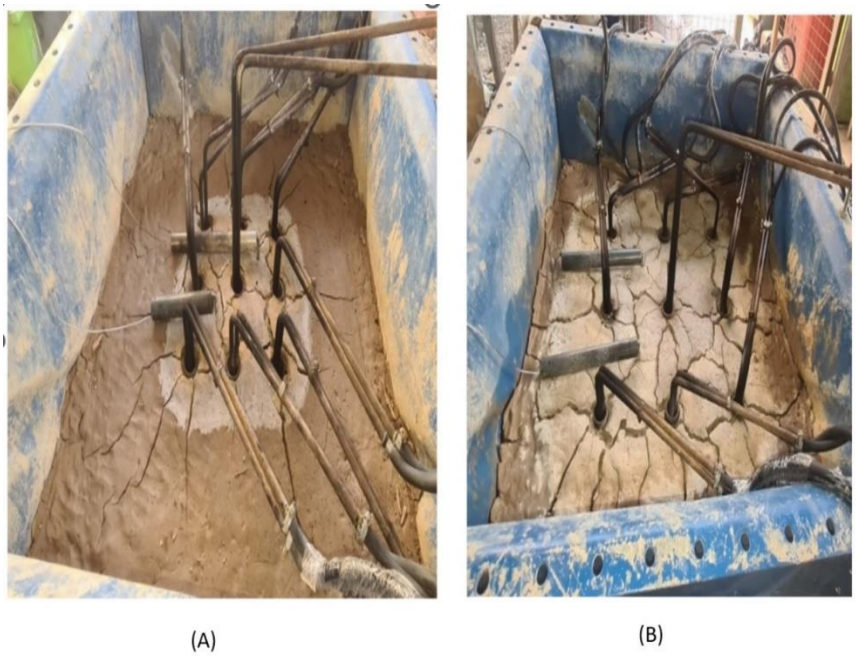

Figure 9. Enhancement area of heating technique: (**A**) the 3D model and (**B**) the 5D model.

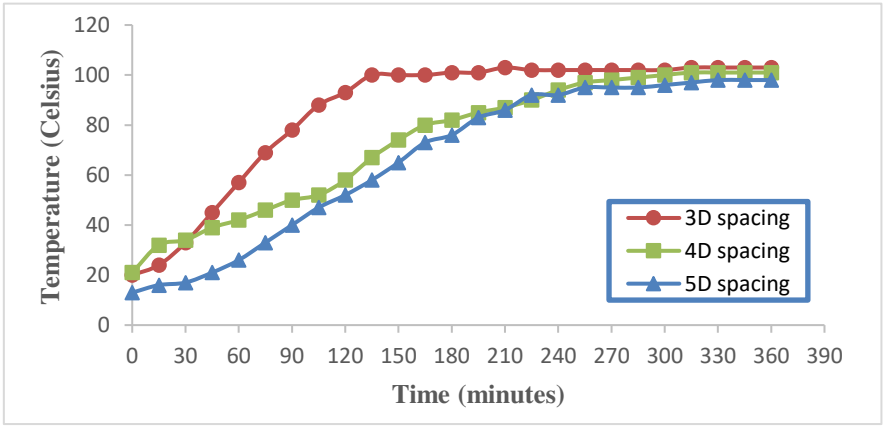

Figure 10. Temperature and duration for the 15 cm thermocable at various spacings.

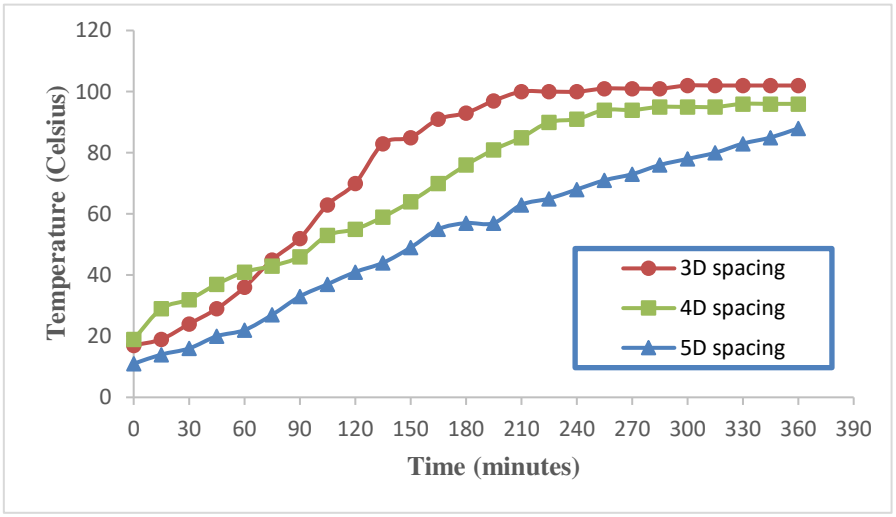

Figure 11. Temperature and duration for the 30 cm thermocable at various spacings.

Preprints (www.preprints.org) | NOT PEER-REVIEWED | Posted: 29 November 2023 doi:10.20944/preprints202311.1881.v1

3.2. Impact of Borehole Casing Depth

Four models with 3D (13 cm) spacing were designed to examine the impact of the borehole casing depth on the bearing capacity. Casing boreholes of varying depths and a square pattern made with nine borehole casings were used to create all the models (b, 1.5b, 2b, and 2.5b), where b is the width of the model footing. There was a standard six-hour heating period for all models. Figure 12 illustrates the dimensionless relationship between the bearing and settlement ratios for all models with various depths, including U.W and U.C. The magnitude of the bearing ratios rises as the borehole casing depth increases. The bearing ratios are 5.03, 5.35, 14.23, 23.57, 27.26, and 28.2 for models U.W, U.C, 1b, 1.5b, 2b, and 2.5b, respectively. The results of all the models are attributed to two factors, depth and area on which the load acted, as illustrated in Figure 13. According to the stress bulb, the stress pressures dissipate with depth, with roughly 40% vanishing at less than 2b depth and 80% at more than 2b depth.

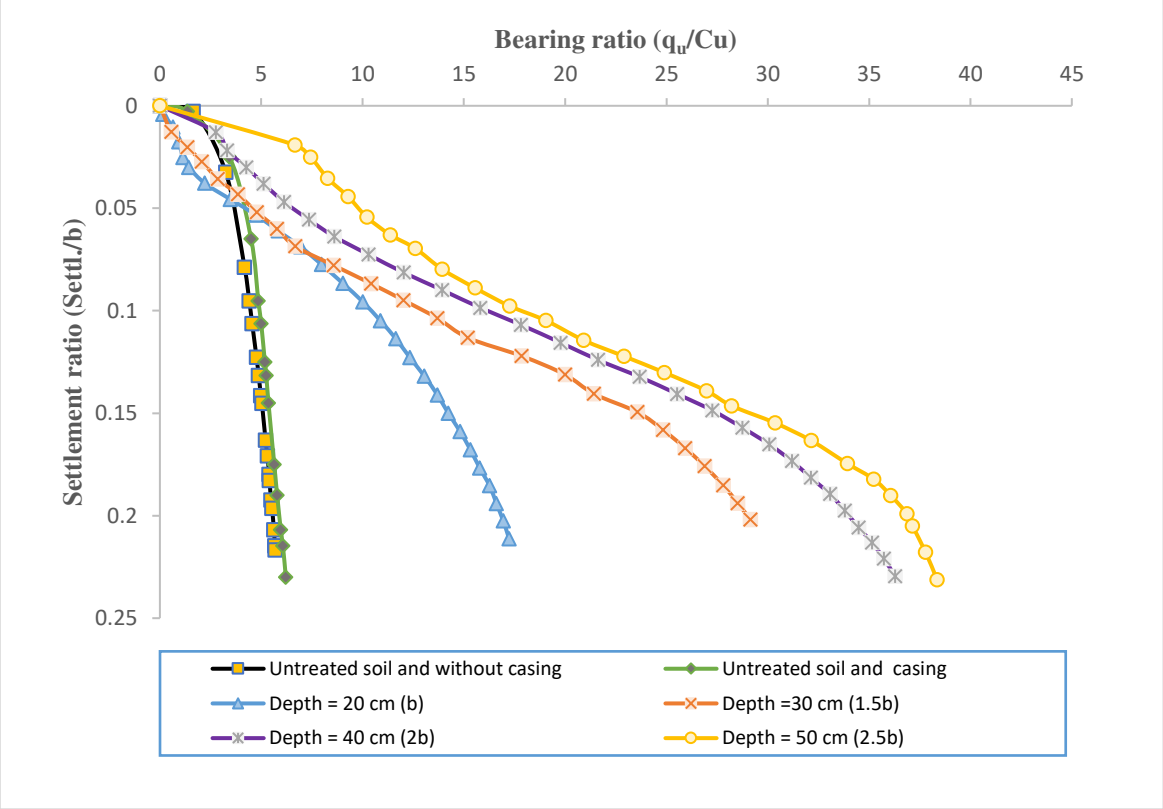

Figure 12. Dimensionless connection between the bearing ratio and the settlement ratio for various depth models.

Preprints (www.preprints.org) | NOT PEER-REVIEWED | Posted: 29 November 2023 doi:10.20944/preprints202311.1881.v1

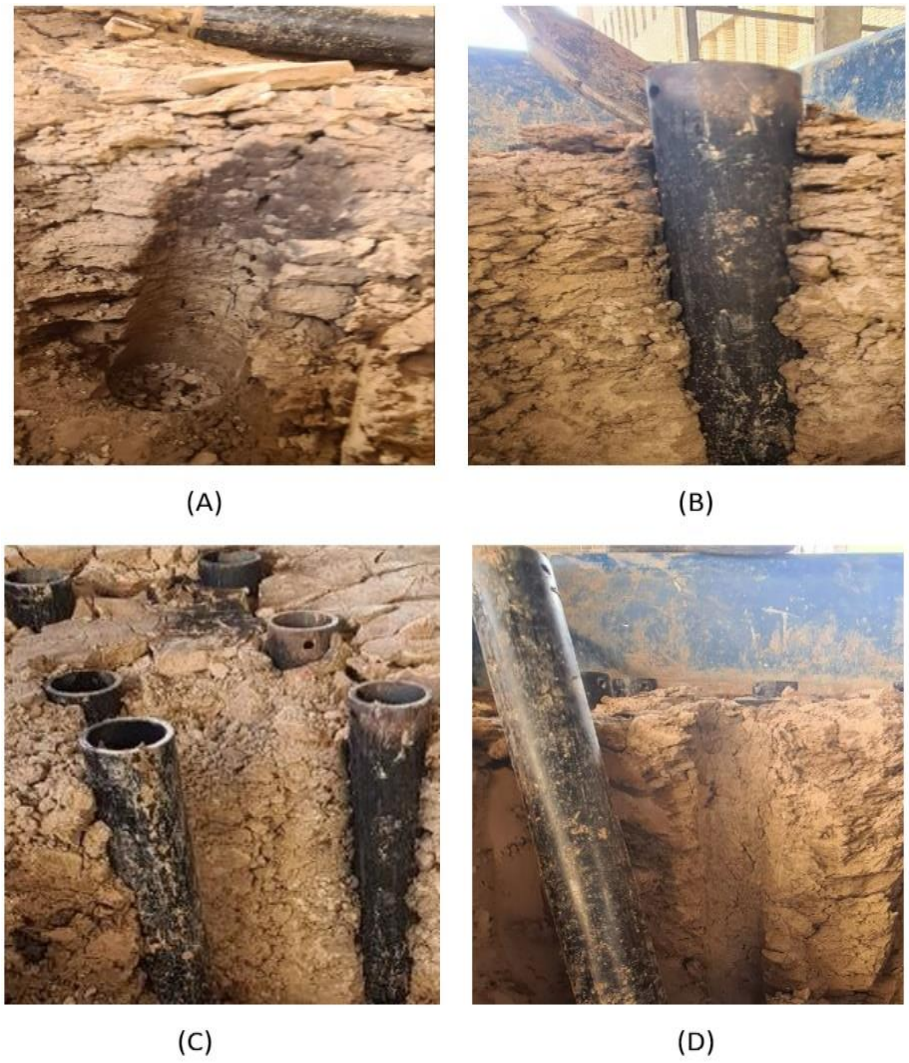

Figure 13. Enhancement area at various depths: (**A**) 20 cm (b), (**B**) 30 cm (1.5b), (**C**) 40 cm (2b), and (**D**) 50 cm (2.5b).

3.3. Impact of Borehole Casing Pattern

To evaluate the pattern effect of the borehole heating casing on the bearing capacity, nine borehole casings with an inner diameter of 3.5 cm, a depth of 40 cm, and a spacing distance of 3D were produced to generate four models with varied patterns (square; circle; triangle (1), with the existence of one borehole heating casing under the footing; and triangle (2), with the existence of two borehole heating casings under the foundation). Figure 14 illustrates the dimensionless relationship between the bearing and settlement ratios for all models with various patterns, including U.W and U.C. At the beginning of the study, the researchers anticipated that the pattern would have a substantial influence; however, as shown in Figure 14, the bearing ratio values are 27.26, 26.19, 23.6, and 23.25 for the model's 3D square, 3D circle, 3D triangle (2), and 3D triangle (1), respectively. In the triangular pattern models, the treated area is not consistent around the footing where the unit cell interlocking is dispersed, and the bearing ratio is low compared to the square pattern models, as seen in Figure 15. As a result of the close proximity between the tiny treated zone and the interlocking unit cells, resulting in the borehole heating casing, the bearing ratio of the circular pattern is lower than that of the square design, as seen in Figure 16. Figures 17 and 18 indicate the temperature fluctuations over time at the midpoint of the treatment zones for the 15 cm and 30 cm thermocables for all models, respectively. Figures 17 and 18 show that the values are varied, most notably in the circular pattern, where the temperature increases to 232 and 160 degrees Celsius. In comparison, it reaches 104 degrees Celsius in the square and rectangular designs at 15 cm and 30 cm thermocable lengths, respectively.

Preprints (www.preprints.org) | NOT PEER-REVIEWED | Posted: 29 November 2023 doi:10.20944/preprints202311.1881.v1

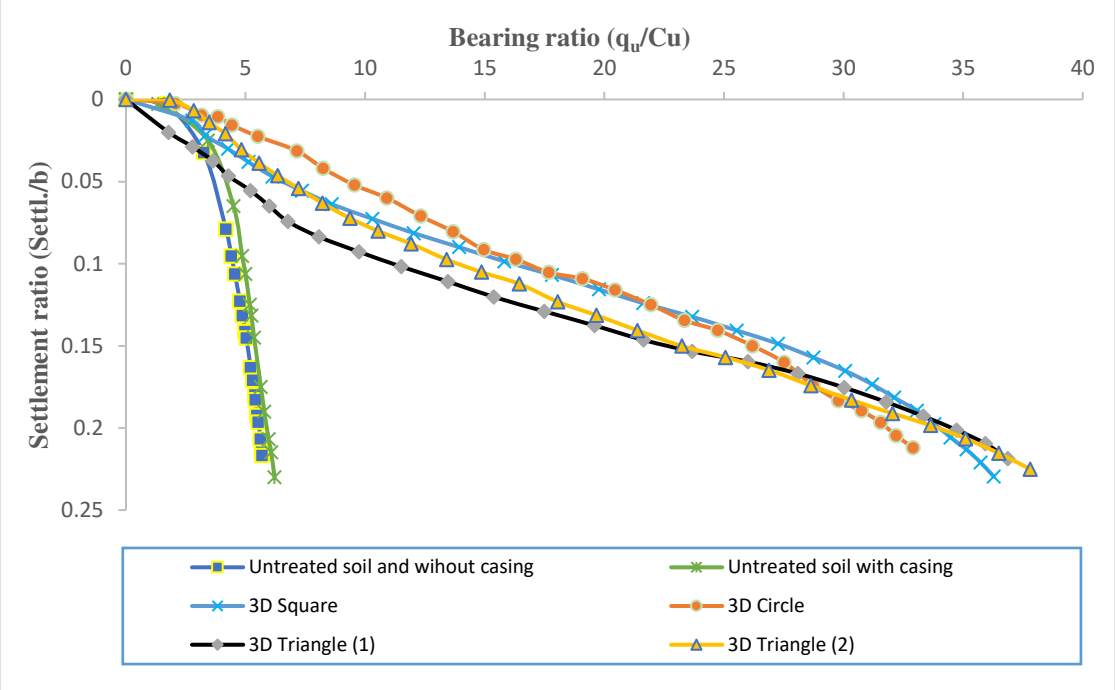

Figure 14. Dimensionless connection between the bearing ratio and the settlement ratio for various pattern models.

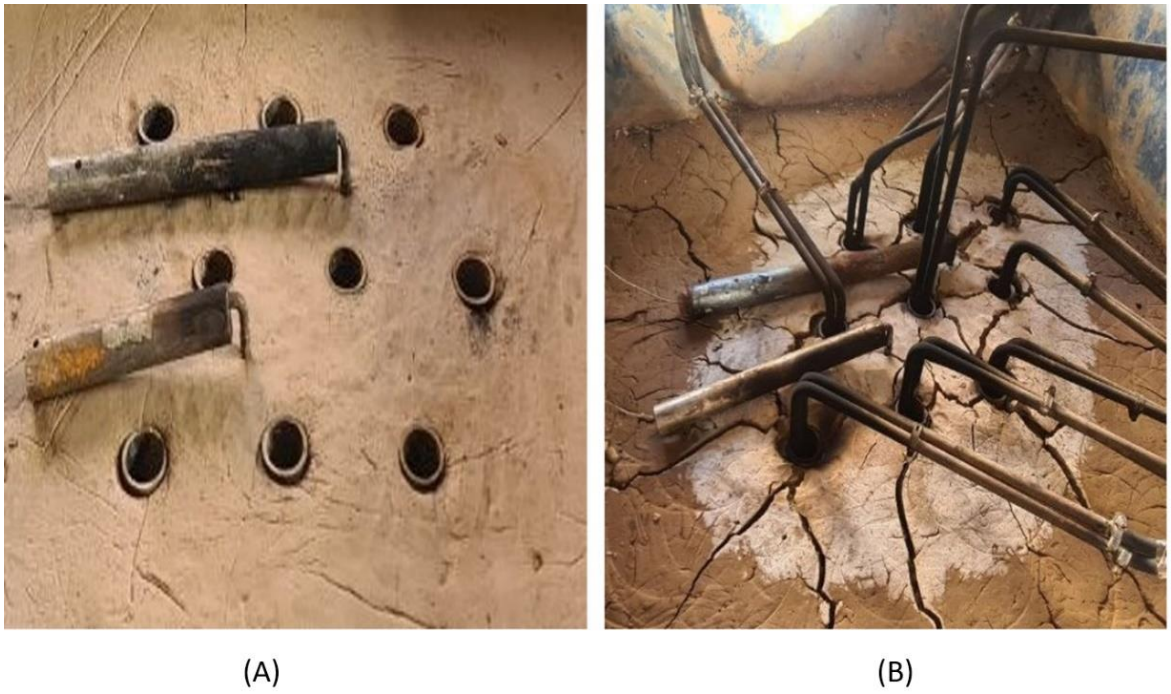

Figure 15. Triangular pattern model: (**A**) triangle (2) (two borehole heating casings under footing), and (**B**) triangle (1) (one borehole heating casing under footing).

Preprints (www.preprints.org) | NOT PEER-REVIEWED | Posted: 29 November 2023 doi:10.20944/preprints202311.1881.v1

Figure 16. Circular pattern model.

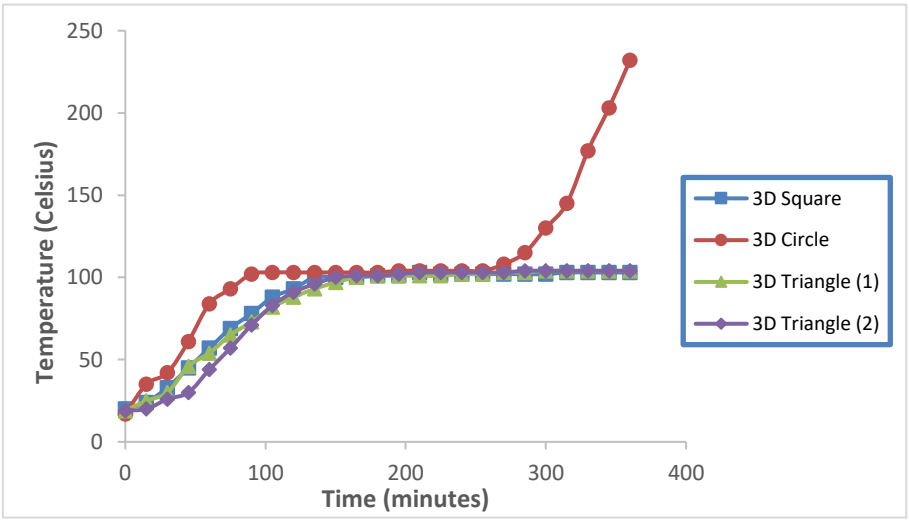

Figure 17. Relationship between temperature and duration for the 15 cm thermocable in various patterns.

Preprints (www.preprints.org) | NOT PEER-REVIEWED | Posted: 29 November 2023 doi:10.20944/preprints202311.1881.v1

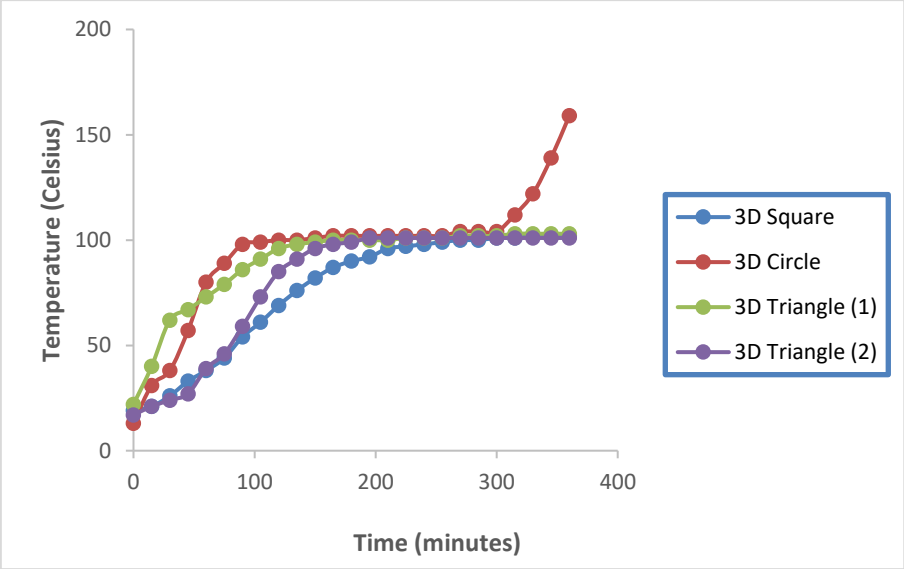

Figure 18. Relationship between temperature and duration for the 30 cm thermocable in various patterns.

3.4. Impact of Heating Time

Five models using the square pattern were created to investigate the impact of heating time on the bearing capacity. The models were heated for varying lengths of time (2, 4, 6, 8, and 10 hrs). The spacing and the extended depth of the borehole casings were 3D and 40 cm (2b), respectively. Figure 19 depicts the dimensionless relationship between the bearing and settlement ratios for all models with varying heating duration ratios. Figure 19 demonstrates that the bearing capacity values rise as the heating duration increases, because the bearing capacity parameters increase when the values of the bearing ratio are 5.03, 5.35, 13.76, 20.9, 27.26, 31.19, and 34.57 for models U.W, U.C, 2 hrs, 4 hrs, 6 hrs, 8 hrs, and 10 hrs, respectively. Significantly, the angle of internal friction where the heating method works on dry soils transforms the clay mineral, which then behaves like sandy soil. Figures 20 and 21 depict the temperature variations with time at the midpoint of the treatment regions at 15 cm and 30 cm of thermocable length for all models, respectively**.** During the first 120 min of heating, the temperature rose rapidly from 21 °C to 98 °C.

The temperature inside the soil model increased until equilibrium was reached at 104 °C, remaining at this temperature for the next four hours. Then, the temperature rose rapidly from 101 °C to 250 °C at 600 min, indicating the occurrence of three distinct phases. In the first stage, the soil and water act as heat conduction bridges. The mixture of soil and water is a uniform heat conductor since the soil particles are entirely covered by water, rapidly increasing the soil's internal temperature. The second stage lasts between 120 and 360 min. The temperature increase is relatively slow until it reaches the equilibrium point of 101 °C. When the temperature rises, the amount of water vapor progressively increases and eventually exits from the soil, causing the soil pores to expand. Heat is transmitted via water, steam, and soil particles as the temperature increases. When all the soil moisture has evaporated, the soil's heat is transported via the soil particles and steam. The stage in which the soil temperature remains at around 101 °C and does not rise due to water vapor is known as the constant stage. After 360 min of heat treatment, the third stage occurs: the water vapor in the soil evaporates entirely, the soil becomes dry, the clay minerals transmit heat fully, and the temperature rises until it exceeds the temperature of the heating source. Thus, it may be concluded that the first and second phases are complete after 360 min, meaning that the soil's water vapor has been released and the soil has become dry. The soil in the study in Ref. [19] exhibits the same conduct. Figure 22 depicts the relationship between the temperature (degrees Celsius) and the horizontal distance of the treatment zone for the 2 hrs, 4 hrs, 6 hrs, 8 hrs, and 10 hrs models, with the peaks on these curves representing the source of heat. Also, due to the action of the heating system, where the

Preprints (www.preprints.org) | NOT PEER-REVIEWED | Posted: 29 November 2023 doi:10.20944/preprints202311.1881.v1

air is pushed into the wells to provide continuous air to run the heating system and remove the trapped gases created by combustion, there is a minor fluctuation in the temperature.

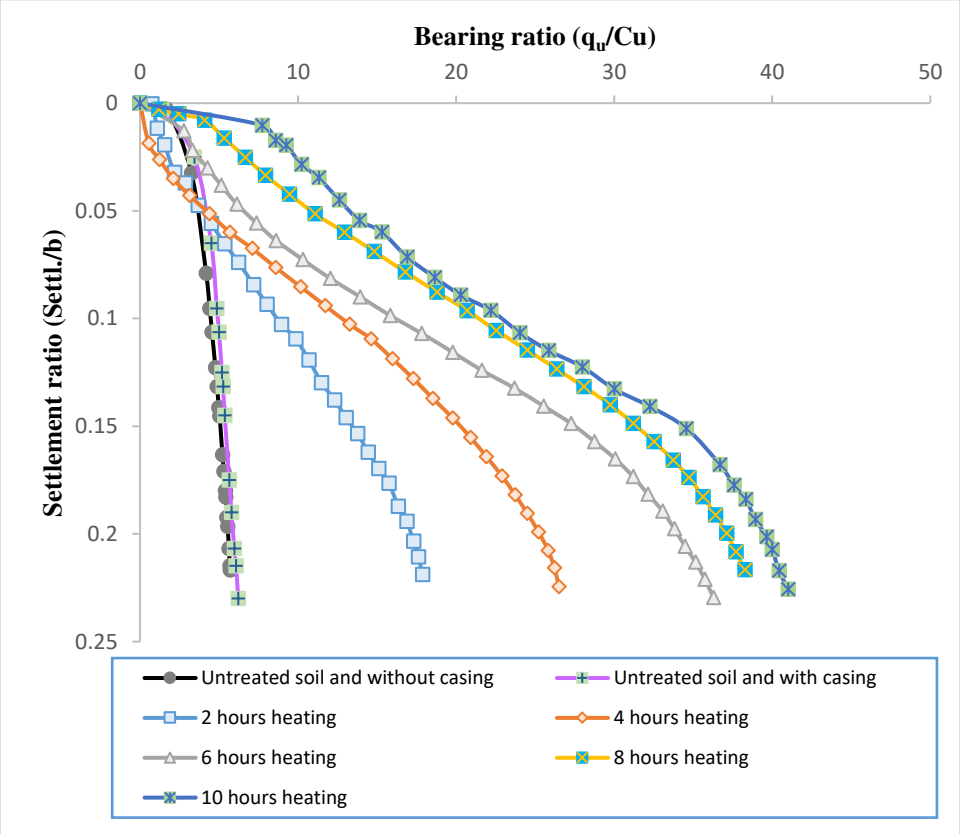

Figure 19. Dimensionless connection between the bearing ratio and settlement ratio for various heating times.

The CPT test was used to determine the increase in undrained shear strength and the angle of internal friction. Four models (CP 1, CP 2, CP 3, and CP 4) were created using the square pattern with 3D distance spacing (13 cm) and a depth of 40 cm for the borehole casing. Figure 23 shows the locations of the CPT test points. The models were heated for 8 hrs. Figures 24–33 show the increase in the undrained shear strength (Cu) and the angle of internal friction (Ø) with regards to the reference model (Cu = 14 kPa and Ø = 0). The increased values of undrained shear strength and angle of internal friction at the center of the heating model (CP 1) occurred from 14 to 360 kPa and 0 to 52 degrees, respectively. However, from the center of the heating model to the furthest point affected by heating (CP 1 to CP 4), the bearing capacity parameter values (Cu and Ø) dropped from 360 to 140 kPa and from 52 to 16 degrees on average with the depth of the heat-treated soil.

Preprints (www.preprints.org) | NOT PEER-REVIEWED | Posted: 29 November 2023 doi:10.20944/preprints202311.1881.v1

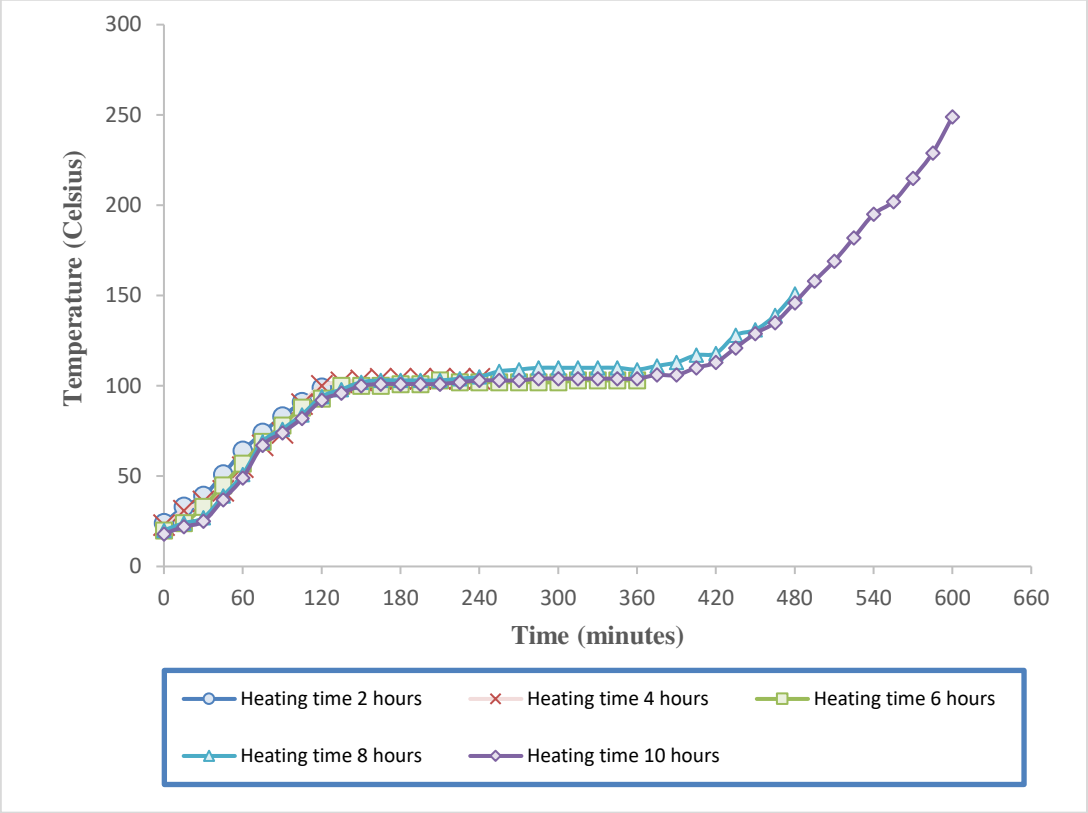

Figure 20. Relationship between temperature and duration for the 15 cm thermocable for various heating times.

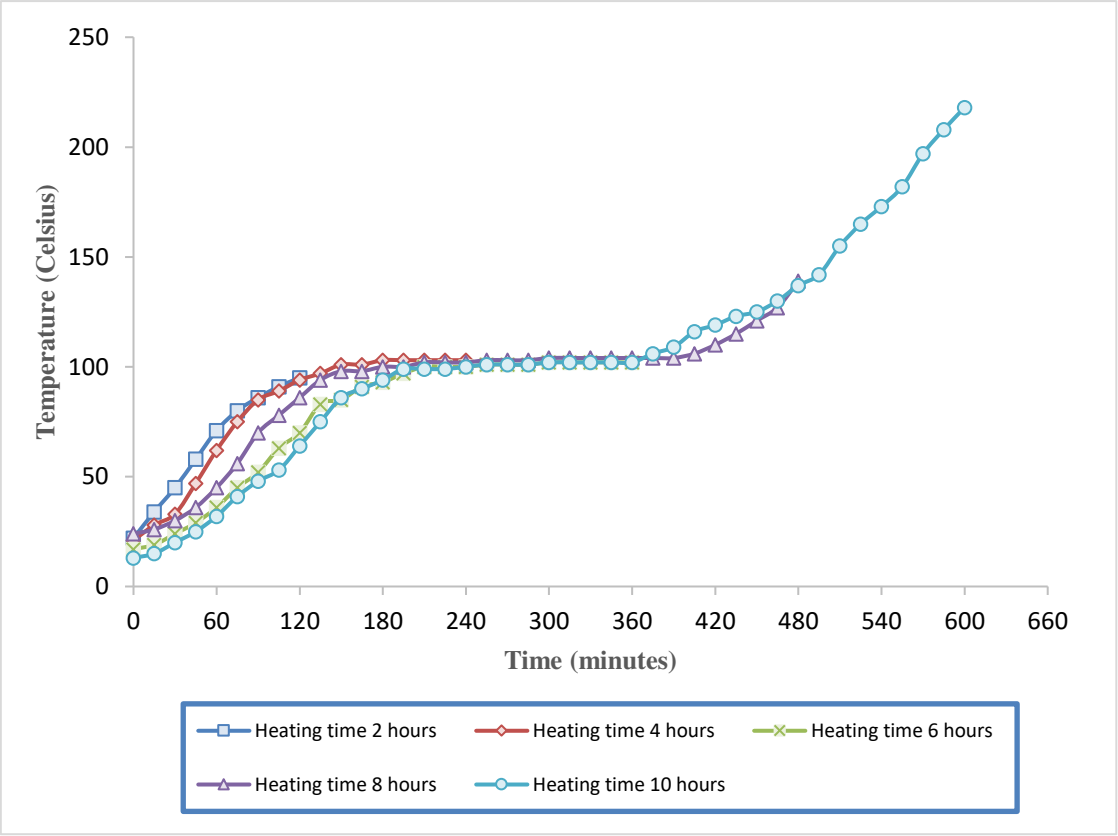

Figure 21. Relationship between temperature and duration for the 30 cm thermocable for various heating times.

Preprints (www.preprints.org) | NOT PEER-REVIEWED | Posted: 29 November 2023 doi:10.20944/preprints202311.1881.v1

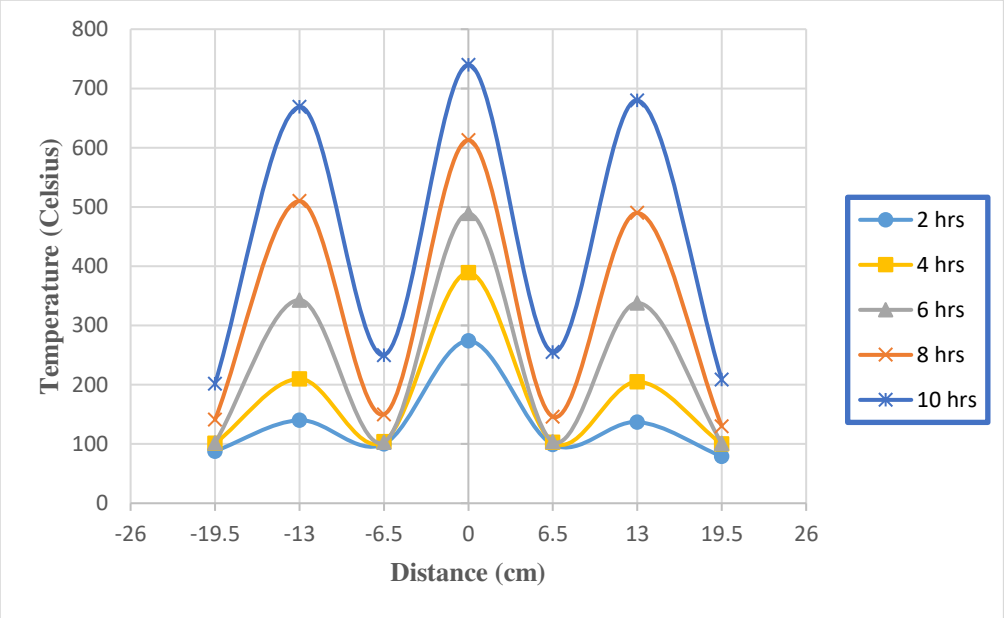

Figure 22. Relationship between temperature and horizontal distance for the 2 h, 4 h, 6 h, 8 h, and 10 h models.

The thermal consolidation effect of the soil was responsible for an increase or decrease in the bearing ratio in the treated soils, where the parameters of bearing capacity, the angle of internal friction, and the undrained shear strength increased or decreased depending on how close or far apart the borehole heating casings were. A rise in the temperature accelerates the movement of suspended particles in the porous medium [18] as well as chemical changes within the treated soil. Figures 34–39 illustrate the EDS (energy-dispersive spectroscopy) pattern for untreated soil and treated soil with different temperature degrees. The specimens used in the EDS test were taken from the physical model's center. Figure 40 illustrates the change in the elemental composition (mg/kg) at different temperatures. The figure shows that as the temperature rises from 100 to 300 °C, the proportions of silicon, aluminum, and iron decrease from 18.04, 5.73, and 6.3 to 10.24, 3.3, and 2.81 (mg/kg), respectively. As the temperature rises to 400 °C, the proportions of these elements increase to 18.28, 6.1, and 5.53, respectively. The increase becomes very small when the temperature reaches 600 °C. However, when the temperature reaches 200 °C, the percentage of calcium increases from 9.18 to 18.36 (mg/kg). If the temperature reaches 400 °C, the percentage of calcium decreases significantly to 13.66 (mg/kg), and when the temperature reaches 600 °C, it decreases even more to 12.21 (mg/kg). When the temperature reaches 300 °C, the percentage of carbon increases from 8.27 to 12.62 (mg/kg), and when the temperature reaches 400 °C, the percentage of this element falls to 7.5 (mg/kg). At this point, the percentage almost stabilizes until the temperature reaches 600 °C. Table 3 includes the elemental composition of the untreated and heat-treated soils.

Preprints (www.preprints.org) | NOT PEER-REVIEWED | Posted: 29 November 2023 doi:10.20944/preprints202311.1881.v1

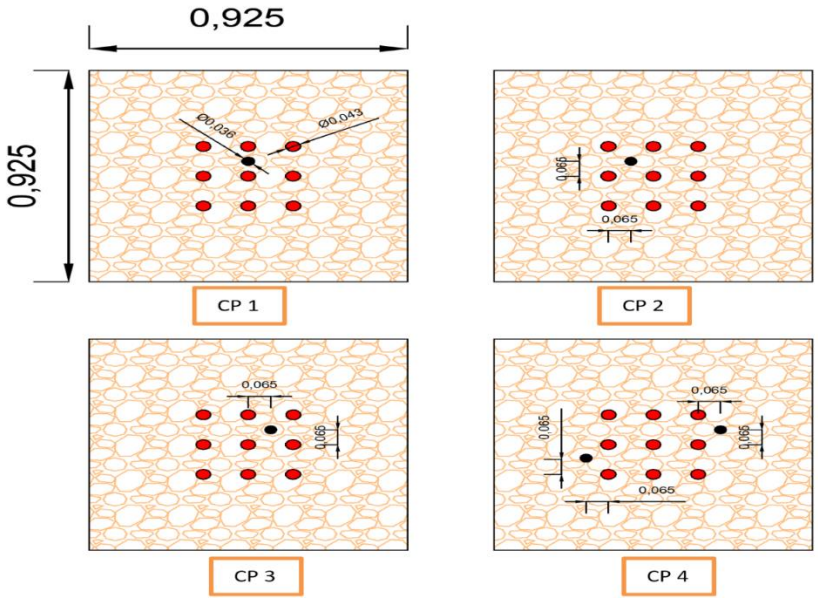

Figure 23. Location of CPT test points (all dimensions in meters).

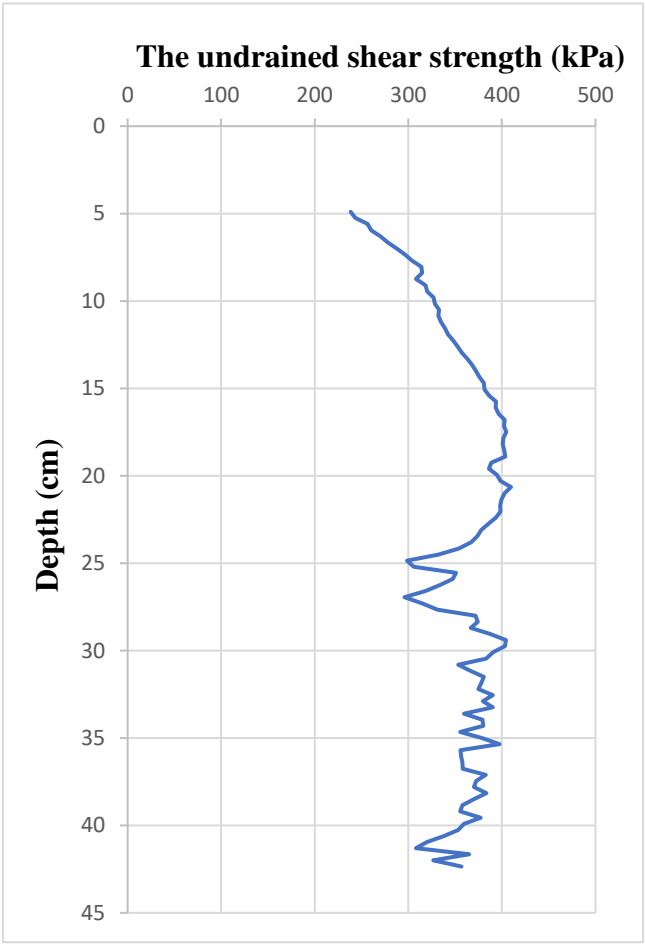

Figure 24. Variation in the undrained shear strength with depth for the CP 1 model.

Preprints (www.preprints.org) | NOT PEER-REVIEWED | Posted: 29 November 2023 doi:10.20944/preprints202311.1881.v1

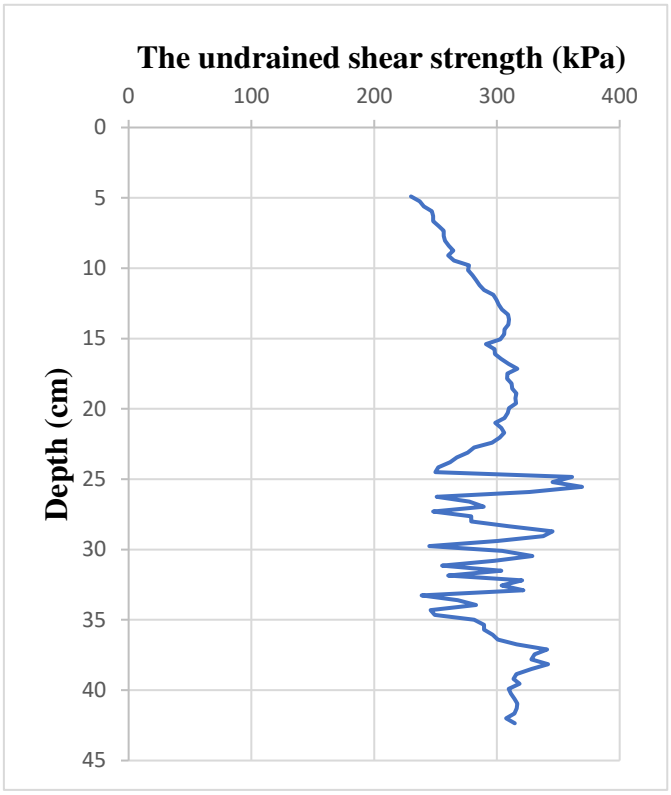

Figure 25. Variation in the undrained shear strength with depth for the CP 2 model.

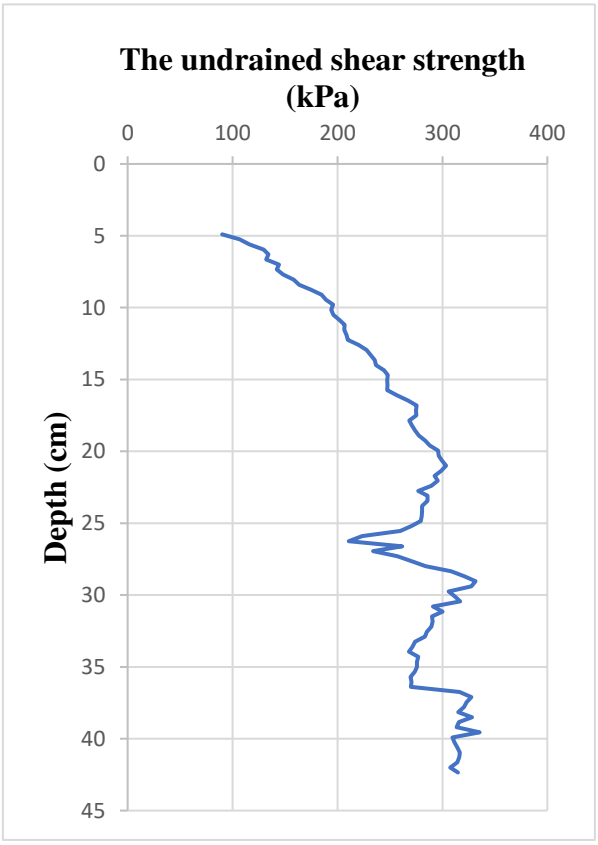

Figure 26. Variation in the undrained shear strength with depth for the CP 3 model.

Preprints (www.preprints.org) | NOT PEER-REVIEWED | Posted: 29 November 2023 doi:10.20944/preprints202311.1881.v1

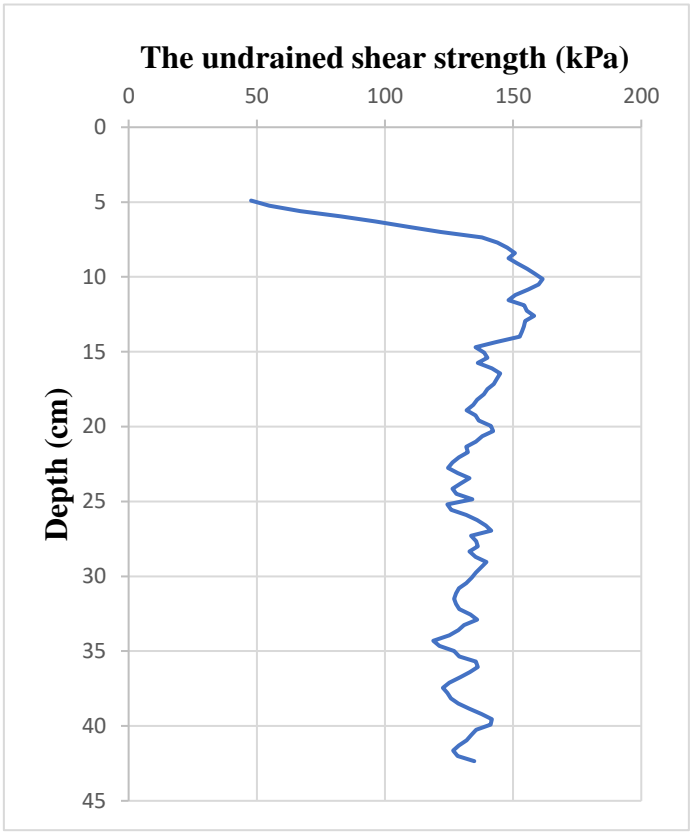

Figure 27. Variation in the undrained shear strength with depth for the CP 4 model (right point).

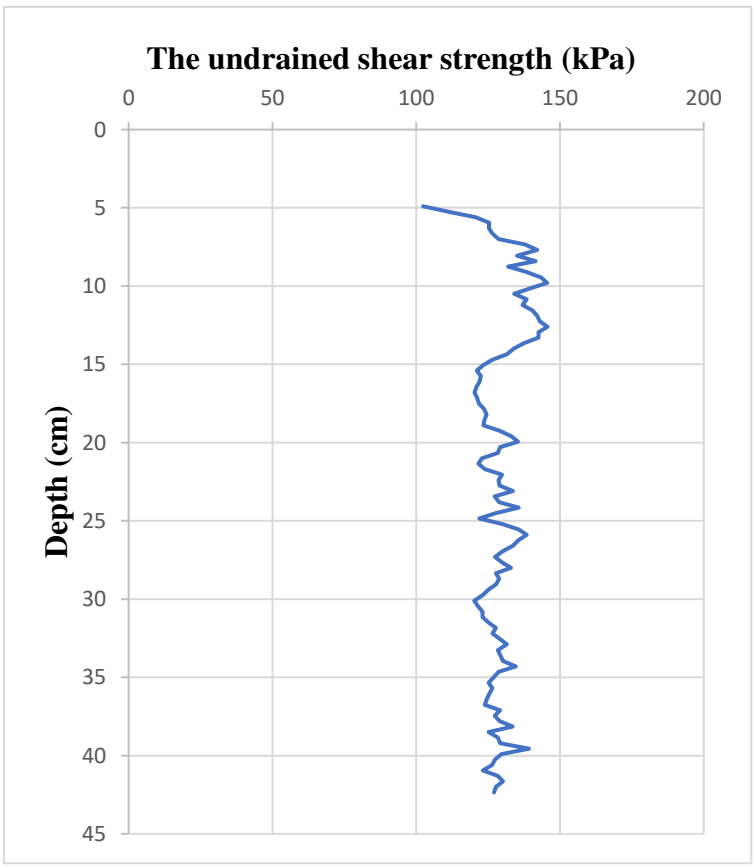

Figure 28. Variation in the undrained shear strength with depth for the CP 4 model (left point).

Preprints (www.preprints.org) | NOT PEER-REVIEWED | Posted: 29 November 2023 doi:10.20944/preprints202311.1881.v1

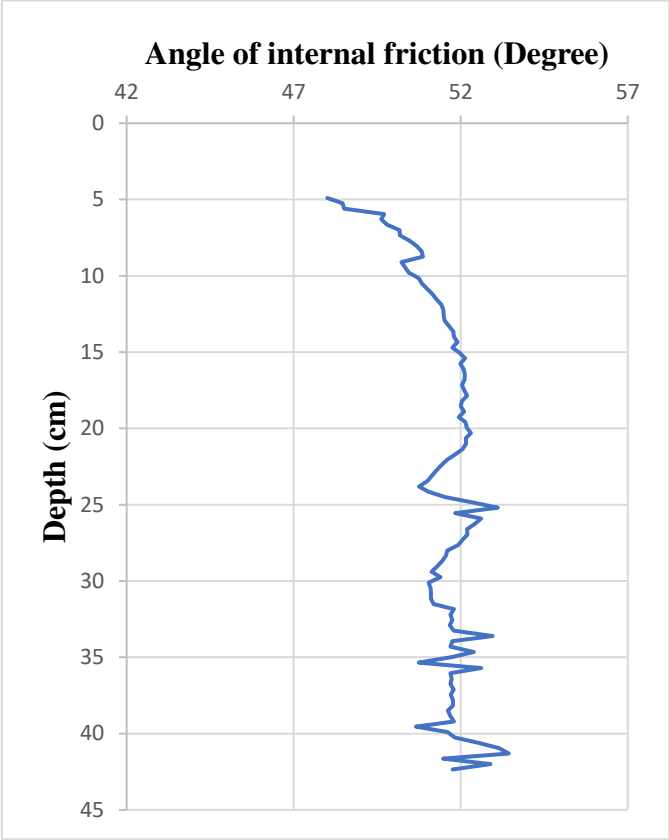

Figure 29. Variation in angle of internal friction (Ø) with depth for the CP 1 model.

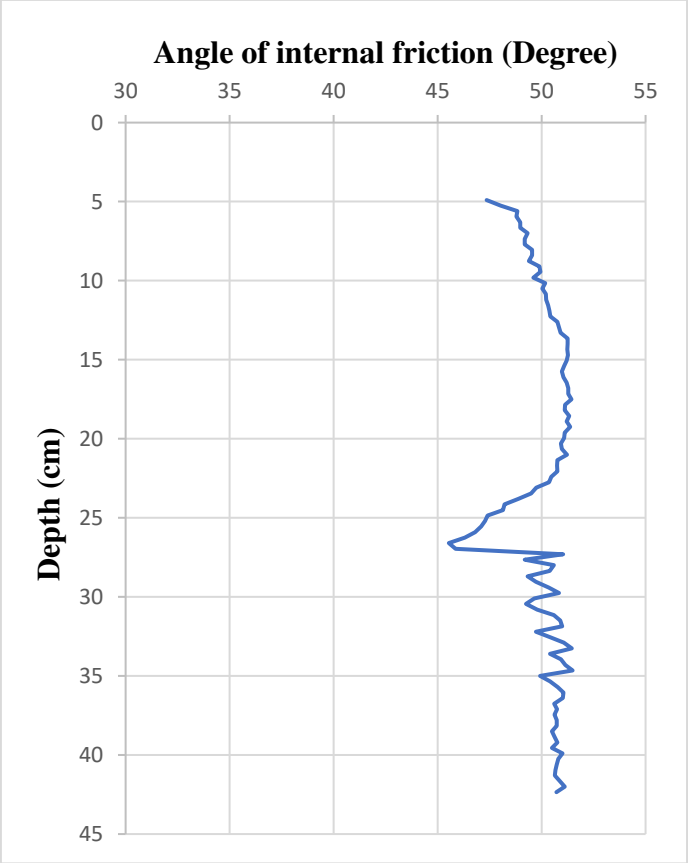

Figure 30. Variation in angle of internal friction (Ø) with depth for the CP 2 model.

Preprints (www.preprints.org) | NOT PEER-REVIEWED | Posted: 29 November 2023 doi:10.20944/preprints202311.1881.v1

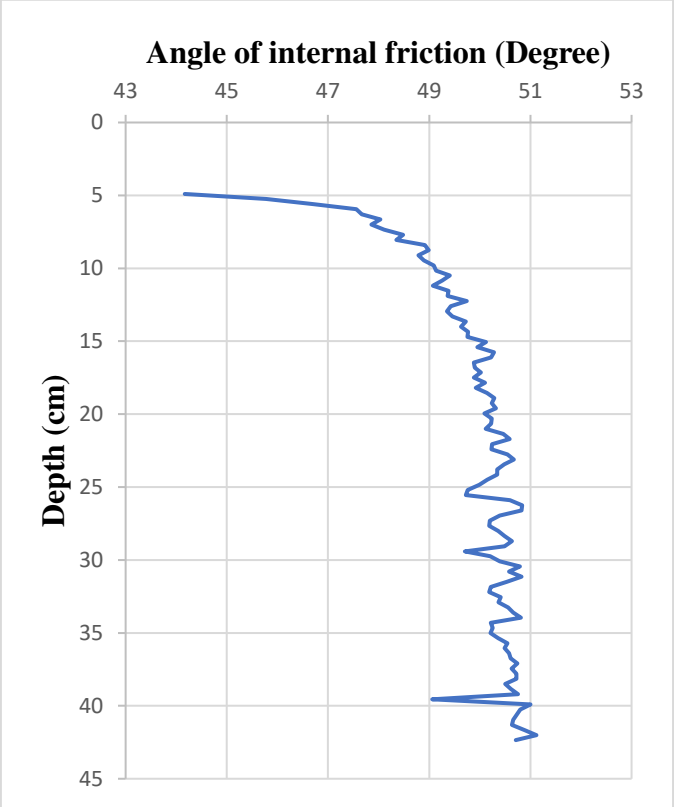

Figure 31. Variation in angle of internal friction (Ø) with depth for the CP 3 model.

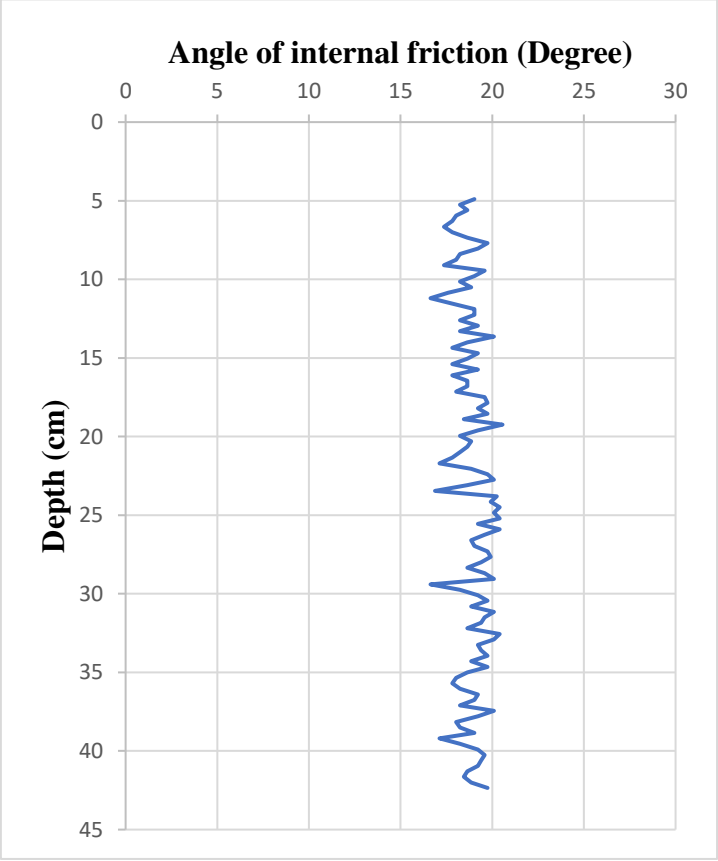

Figure 32. Variation in angle of internal friction (Ø) with depth for the CP 4 model (right point).

Preprints (www.preprints.org) | NOT PEER-REVIEWED | Posted: 29 November 2023 doi:10.20944/preprints202311.1881.v1

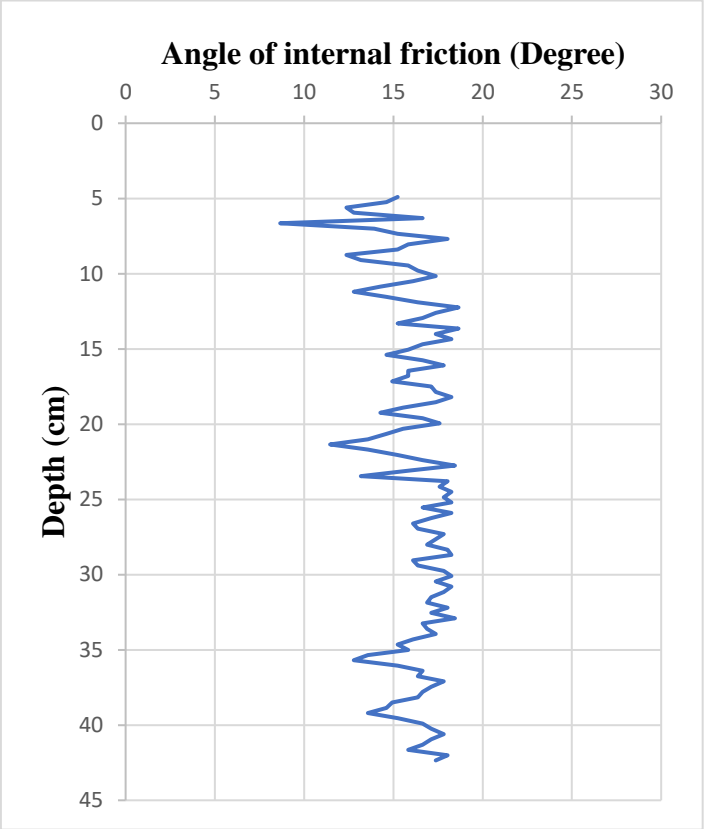

Figure 33. Variation in angle of internal friction (Ø) with depth for the CP 4 model (left point).

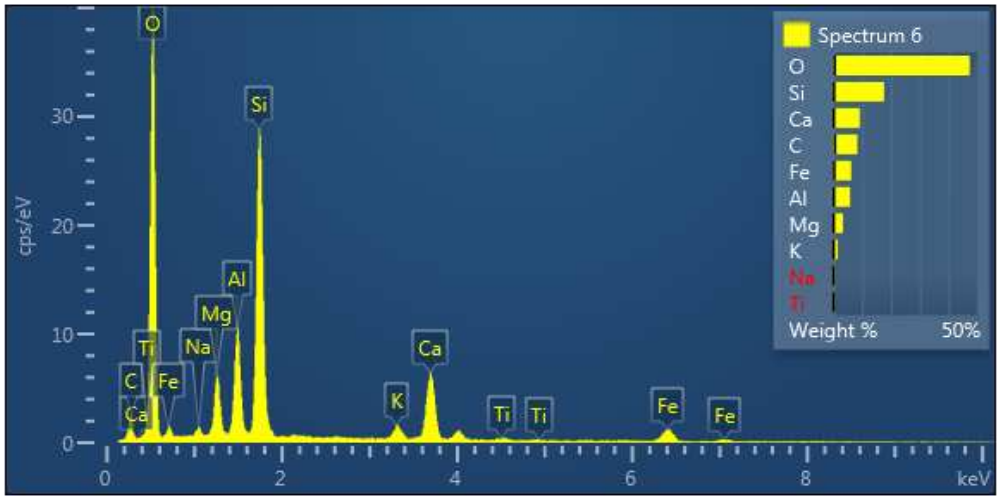

Figure 34. EDS pattern for untreated soil.

Preprints (www.preprints.org) | NOT PEER-REVIEWED | Posted: 29 November 2023 doi:10.20944/preprints202311.1881.v1

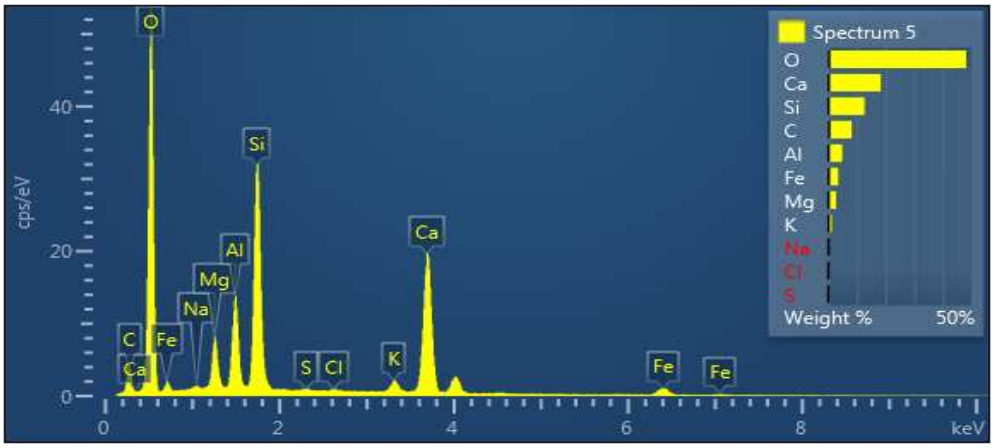

Figure 35. EDS of soil treated at 200 °C.

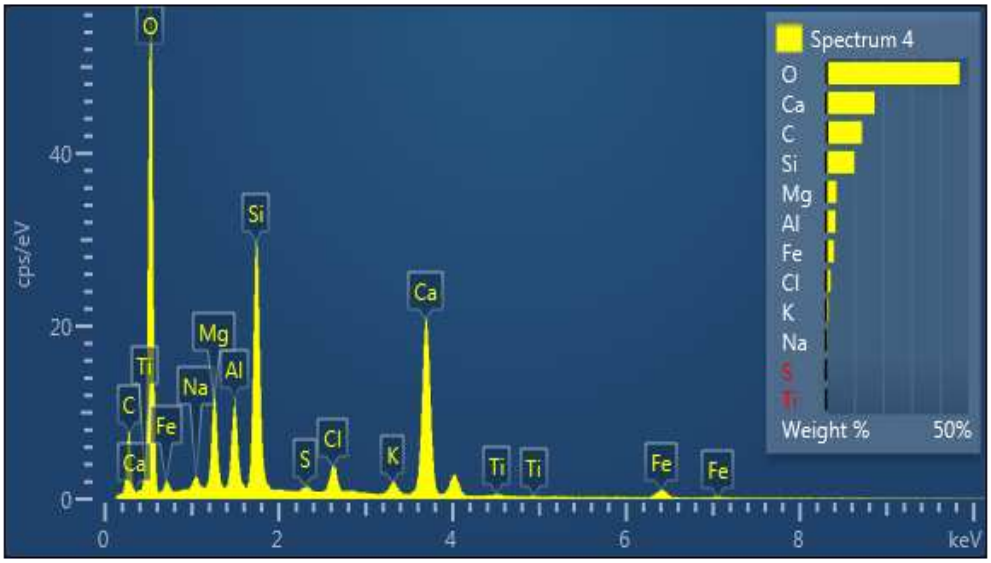

Figure 36. EDS of soil treated at 300 °C.

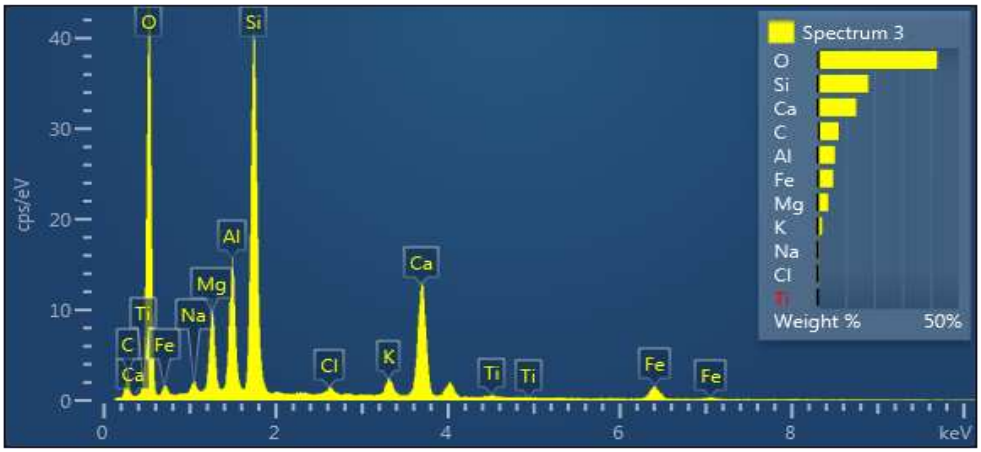

Figure 37. EDS of soil treated at 400 °C.

Preprints (www.preprints.org) | NOT PEER-REVIEWED | Posted: 29 November 2023 doi:10.20944/preprints202311.1881.v1

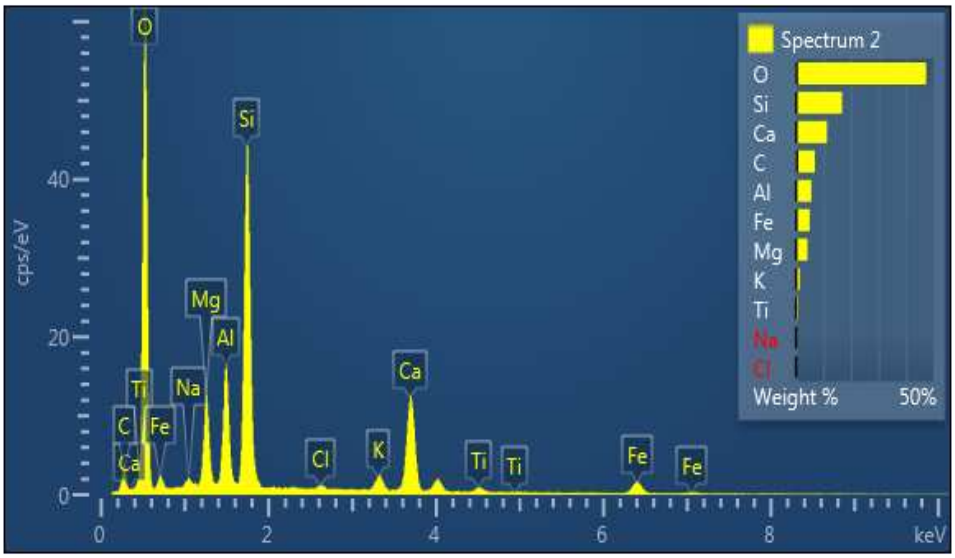

Figure 38. EDS of soil treated at 500 °C.

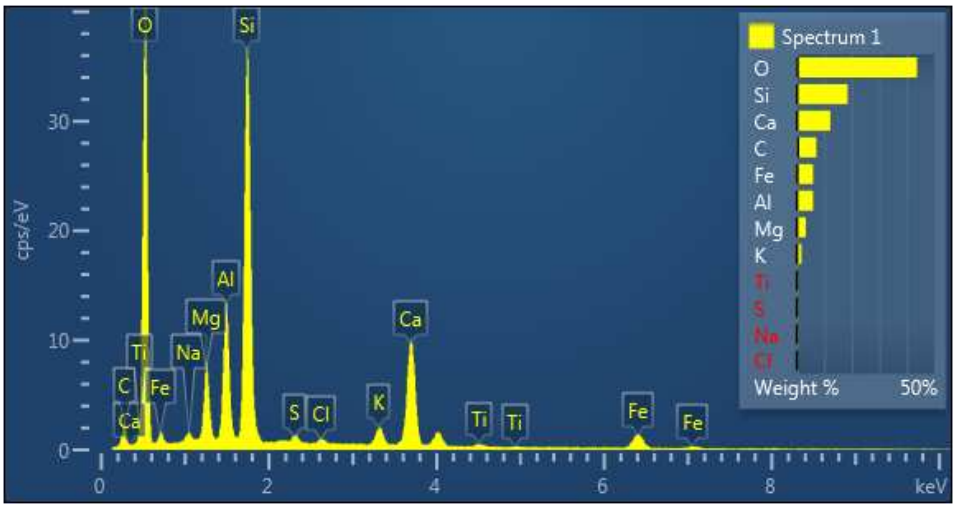

Figure 39. EDS of soil treated at 600 °C.

Table 3. Elemental composition (from EDS analysis) of the untreated soil and treated soil.

Element	Untreated Soil	Treated Soil at 200 °C	Treated Soil at 300 °C	Treated Soil at 400 °C	Treated Soil at 500 °C	Treated Soil at 600 °C
	Weight (mg/kg)	Weight (mg/kg)	Weight (mg/kg)	Weight (mg/kg)	Weight (mg/kg)	Weight (mg/kg)
Si	18.04	12.68	10.24	18.28	18.84	18.89
O	47.39	47.26	46.37	42.29	42.91	43.69
Al	5.73	4.88	3.3	6.1	5.96	5.94
C	8.27	8.16	12.62	7.5	6.91	7.08
Ca	9.16	18.36	17.08	13.66	12.96	12.21
Na	0.53	0.15	0.56	0.62	0.39	0.41
K	1.48	1.19	0.96	1.66	1.67	1.69
Fe	6.13	3.44	2.81	5.53	5.61	5.95
Mg	3.27	2.7	3.63	3.77	4.17	3.3
S	0	0.11	0.27	0	0	0.44
Cl	0	0.12	1.67	0.52	0.28	0.36

Preprints (www.preprints.org) | NOT PEER-REVIEWED | Posted: 29 November 2023 doi:10.20944/preprints202311.1881.v1

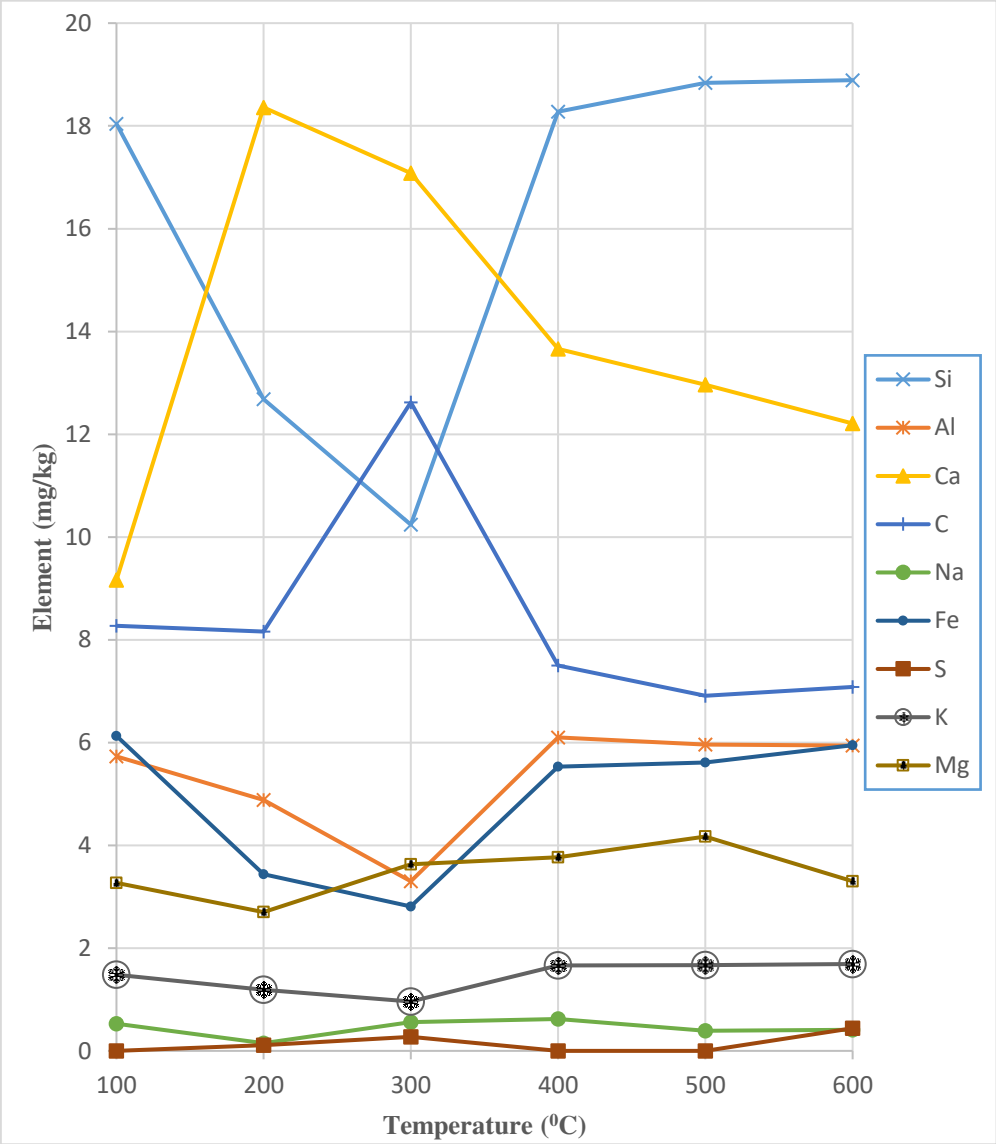

Figure 40. Change in elemental composition (mg/kg) at different temperatures.

4. Conclusions

Based on the findings of the current research, the following inferences can be obtained:

1. The bearing ratio reduces from 27.26 to 21.78 at a 15% settlement ratio if the spacing increases from 3D to 5D. The interlocking between unit cells is significant and reduces the temperature in the center of the treated zone.
2. At a 15% settlement ratio, the magnitude of the bearing ratio rises from 14.23 to 28.2 for models 1b to 2.5b as the borehole casing depth increases. Also, this substantial increase gradually reduces from 27.26 to 28.2 for models 2b to 2.5b.
3. The effect of the pattern is small when the borehole heating casing is used. The bearing ratio is 26.19 for the circle pattern model, while the bearing ratio for the square pattern model is higher at 27.26. The amount of heat gained determines the strength of the treated area. The greater the amount of heat in the footing center, the greater the strength of the heat-treated zone. Also, increasing the strength is the correct distribution of the borehole heating casing, which provides an appropriate treatment area according to the order of the stresses applied mainly to the treatment area consisting of interlocking unit cells.
4. The bearing ratio value increases from 13.76 to 34.57 for 2–10 h heating duration models at a 15% settlement ratio. A small increase in the bearing ratio, from 31.19 to 34.57, is observed for 8–10 h

heating duration models. Also, the rate of improvement rises rapidly for the first six hours, but diminishes after that.

5. The best spacing between boreholes is three times the outer diameter of the borehole, and the best borehole depth is two times the width of the foundation footing with 8 h of heating duration.
6. The values of the undrained shear strength and angle of internal friction at the center of the heating model (CP 1) increase from 14 to 360 kPa and 0 to 52 degrees, respectively.
7. The EDS pattern for the treated soils demonstrates that the percentage of elements such as silicon, aluminum, and iron decreases at 300 °C and increases at 400 °C. Moreover, the percentage of calcium increases as the temperature reaches 200 °C and sharply decreases when it reaches 400 °C. The amount of carbon increases as the temperature rises to 300 °C and decreases at 400 °C.
8. The amounts of the measured elements exhibit either low or negligible fluctuations when the temperature falls within the range of 400 °C to 600 °C.

Author Contributions:. Ali H. Shareef: Conceptualization, Carrying out experimental research, Writing – review & editing; Mohammed A. Al- Neami: Writing – review & editing, Supervision; Falah H. Rahil: Writing – original draft, Supervision.

Funding: This research received no specific grant from any funding agency in the public, commercial, or not-for-profit sectors.

Data Availability Statement: The data that support the findings of this study are available on request from the corresponding author.

Conflicts of Interest: The authors declare that there is no conflict of interest.

References

1. Al-Neami, M.A.M. Reducing settlement of soft soils using local materials. *Eng. Technol. J.* **2010**, *28*, 6649–6661.
2. Sasanian, S. *The Behaviour of Cement Stabilised Clay at High Water Contents*; The University of Western Ontario: London, ON, Canada, 2011.
3. Ahmed, A. Compressive strength and microstructure of soft clay soil stabilised with recycled bassanite. *Appl. Clay Sci.* **2015**, *104*, 27–35.
4. Sukpunya, A.; Jotisankasa, A. Large simple shear testing of soft Bangkok clay stabilised with soil–cement-columns and its application. *Soils Found.* **2016**, *56*, 640–651.
5. Tan, Ö.; Yılmaz, L.; Zaimoğlu, A.S. Variation of some engineering properties of clays with heat treatment. *Mater. Lett.* **2004**, *58*, 1176–1179.
6. Abu-Zreig, M.M.; Al-Akhras, N.M.; Attom, M.F. Influence of heat treatment on the behavior of clayey soils. *Appl. Clay Sci*. **2001**, *20*, 129–135.
7. Sun, Q.; Zhang, W.; Qian, H. Effects of high temperature thermal treatment on the physical properties of clay. *Environ. Earth Sci.* **2016**, *75*, 610.
8. Geng, J.; Sun, Q. Effects of high temperature treatment on physical-thermal properties of clay. *Thermochim. Acta* **2018**, *666*, 148–155.
9. Hu, Q.; Gu, Y.; Zeng, J.; He, L.; Tang, H.; Wei, G.; Lu, X. Microwave irradiation reinforcement of weak muddy intercalation in slope. *Appl. Clay Sci.* **2019**, *183*, 105324.
10. Zhang, S.; Ding, Y.; Lu, X.; Mao, X.; Song, M. Rapid and efficient disposal of radioactive contaminated soil using microwave sintering method. *Mater. Lett*. **2016**, *175*, 165–168.
11. Chen, Z.; Zhu, H.; Yan, Z.; Zhao, L.; Shen, Y.; Misra, A. Experimental study on physical properties of soft soil after high temperature exposure. *Eng. Geol.* **2016**, *204*, 14–22.
12. Yin, T.; Liu, G.; Guo, Z. Theoretical and experimental study on thermal consolidation characteristics of typical soft clay in Ningbo region. *Build. Struct.* **2014**, *44*, 66–69.
13. Chen, Y.; Sun, Z.; Cui, Y.; Ye, W.; Liu, Q. Effect of cement solutions on the swelling pressure of compacted GMZ bentonite at different temperatures. *Constr. Build. Mater.* **2019**, *229*, 116872.
14. Reinosa, J.J.; García-Baños, B.; Catalá-Civera, J.M.; Fernández, J.F. A step ahead on efficient microwave heating for kaolinite. *Appl. Clay Sci.* **2019**, *168*, 237–243.
15. Yao, H.; Lu, J.; Bian, H.; Zhang, Z. Influence of microwave heating on the swelling properties of expansive soil in Hefei. *Case Stud. Therm. Eng.* **2022**, *39*, 102466.
16. Demirbas, A. Fuel properties of hydrogen, liquefied petroleum gas (LPG), and compressed natural gas (CNG) for transportation. *Energy Sources* **2002**, *24*, 601–610.
17. Rahil, F.; Baqir, H.; Alkabee, H. Bearing capacity of soft clay improved by heating through different spacing cased boreholes. *Kufa J. Eng.* **2019**, *10*, 68–77.

18. Bai, B.; Long, F.; Rao, D.; Xu, T. The effect of temperature on the seepage transport of suspended particles in a porous medium. *Hydrol. Process*. **2017**, *31*, 382–393.
19. Zhu, H.; Chen, Z.; Wang, Y.; Yan, Z. Experimental investigation on heat transfer characteristics of soft clay at high temperatures. *Jpn. Geotech. Soc. Spec. Publ.* **2015**, *1*, 40–44.